The effect of anode support on the electrochemical performance of microtubular solid oxide fuel cells fabricated by gel-casting

M. Morales [1,2,*], M.A. Laguna-Bercero[3], M.E. Navarro[4], F. Espiell[1], M. Segarra[1]

[1] Centre DIOPMA, IN2UB, Departament de Ciència dels Materials i Enginyeria Metal·lúrgica. Universitat de Barcelona, Martí i Franquès 1, 08028 Barcelona (Spain).

[2] DIOPMA, S.L., Parc Científic de Barcelona, Baldiri i Reixach, 10, Edificio Clúster, 08028 - Barcelona (Spain).

[3] Instituto de Ciencia de Materiales de Aragón, CSIC-Universidad de Zaragoza, C/ Pedro Cerbuna 12, 50009 - Zaragoza (Spain).

[4] School of Chemical Engineering, University of Birmingham, Edgbaston, B15 2TT - Birmingham (United Kingdom).

.

* Corresponding author:

E-mail address: mmorales@ub.edu; mmoralescomas@yahoo.es

Tel.: +34 934021316; fax: +34 934035438

Abstract

Different cell configurations of anode-supported microtubular solid oxide fuel cells (mT-SOFCs) using samaria-doped ceria (SDC) as the electrolyte were fabricated. Different cells were processed varying the porosity and wall thickness-(outer diameter) of NiO-SDC tubular supports. Suitable aqueous slurry formulations of NiO-SDC for gel-casting were prepared using agarose, as a gelling agent, and sucrose, as a pore former. The subsequent NiO-SDC anode functional layer (AFL), the SDC electrolyte and the $La_{0.6}Sr_{0.4}Co_{0.2}Fe_{0.8}O_{3-d}$-SDC cathode were deposited by spray-coating. Pre-sintering temperatures of the supports were optimized from linear shrinkage curves, thus obtaining after co-sintering, a dense electrolyte without anode-electrolyte delamination. Electrochemical characterization of mT-SOFC cells fabricated by agarose gel-casting is reported by the first time. The cell with a support of 2.6 mm diameter, 380 μm wall

thickness, an active area of 1 cm^2 and added porosity, using 10 wt.% sucrose, achieved a maximum power density of about 400 mW·cm^{-2} at 650°C.

Keywords: Anode-supported; Solid Oxide Fuel Cells; Microtubular; Doped ceria; Gel-casting.

1 Introduction

Solid oxide fuel cells (SOFCs) are electrochemical energy conversion devices applicable from portable systems of a few watts up to megawatt-sized power plants with high efficiency and low emissions of pollution [1,2]. Portable applications for SOFCs are envisaged in the fields of Auxiliary Power Units (APU) in transport, small power units for personnel, submarines, air planes, etc. Tubular SOFC designs have demonstrated to be effective for portable devices, since they possess high thermal shock resistance, less stringent sealing requirements, and a low thermal stress caused by rapid heating up to the operating temperature [3,4]. By decreasing the cell diameter to a few millimetres or sub-millimetres, such as mT-SOFCs, it is possible to improve the mechanical stability, thermo-cycling resistance, volumetric power density, and also to reduce start-up times [5,6,7,8,9]. In addition, mT-SOFCs operating at intermediate temperatures (500-700ºC) are desirable to decrease the material degradation and to reduce costs by incorporating metallic materials [10]. For this purpose, both decreasing the electrolyte thickness to reduce ohmic resistance losses and using based electrolytes on gadolinium doped ceria (GDC), samarium doped ceria (SDC), or strontium and magnesium doped LaGaO$_3$ perovskite (LSGM), which present high ionic conductivity at intermediate temperatures, are good approaches [11,12,13].

In contrast, the manufacturing of mT-SOFCs is the main disadvantage in comparison to the planar design, as it is more difficult to fabricate a tight electrolyte layer deposited on a porous substrate in the tubular geometry. For this reason, processing methods are

one of the most important topics in microtubular SOFC research, which present several difficulties, such as a relatively high investment in equipment and a long time for the adjustment of processing parameters. The most typical techniques for the support processing include cold isostatic pressing [14,15], slip-casting [16], extrusion [17], electrophoretic deposition [18] and co-extrusion [19] amongst others. Alternatively, aqueous gel-casting is a wet-forming technique that allows to prepare dense and porous ceramics, with high quality and complex geometry, in short forming times, and low-cost equipments [20,21,22]. For example, it can be used to shape the tubular cell both at laboratory and industry scale [23,24,25]. Owing to the toxicity of some synthetic monomers, natural polysaccharides, such as agar and agarose, have been used as gelling agents [23,26]. These form a gel on cooling, thus exhibiting large similarities to the principles of injection moulding. Recently, Morales et al. [27,28] have reported a new methodology combining the agarose gel-casting and spray-coating techniques that are easily industrially scalable for processing the anode-supported tubular cells based on $NiO\text{-}Sm_{0.2}Ce_{0.8}O_{1.9}/Sm_{0.2}Ce_{0.8}O_{1.9}/La_{0.5}Sr_{0.5}CoO_{3\text{-}\delta}\text{-}Sm_{0.2}Ce_{0.8}O_{1.9}$ (Ni-SDC/SDC/LSC-SDC). Tubular supports were shaped by a gel-casting method based on a new and simple forming technique, which operates as a syringe.

Despite the advantages of the agarose gel-casting technique, only a few works have employed this method for processing of the anode-supported tubular SOFCs. Dong et al. reported mT-SOFCs using yttria-stabilized zirconia (YSZ) as the electrolyte [25]. Our group recently reported the manufacturing of samaria-doped ceria based microtubular cells by the gel-casting technique [27,28]. However, no electrochemical result was previously reported. In addition, the effects of the porosity and wall thickness of gel-casted tubular supports on the cell performance have not been previously studied, which are particularly crucial to successfully implement a new shaping method for mT-SOFCs. The purpose of this study is to fabricate anode-supported mT-SOFCs with SDC electrolyte by combining the agarose gel-casting and spray-coating

techniques, emphasizing the effects of the porosity and wall thickness-(outer diameter) of supports on the cell performance. In order to optimize the manufacturing parameters, the formulation of suspensions, using sucrose as pore former, and the pre-sintering process of supports has been investigated.

2 Experimental procedure

2.1 Material synthesis

Samarium-doped ceria, nickel oxide-samarium doped ceria , and lanthanum strontium cobaltite powders, with a nominal composition of $Sm_{0.2}Ce_{0.8}O_{1.9}$ (SDC), NiO-$Sm_{0.2}Ce_{0.8}O_{1.9}$ (60:40 and 50:50 wt.% NiO-SDC) and $La_{0.6}Sr_{0.4}Co_{0.2}Fe_{0.8}O_{3-\delta}$ (LSCF) respectively, were synthesized by polyacrylamide gel combustion as described elsewhere [29,30]. The materials were prepared from Sm_2O_3 (Strem Chemical 99.9%), CeO_2 (Strem Chemical 99.9%), La_2O_3 (Alfa Aesar 99.9%), $Sr(CH_3COO)_2$ (Pro-BVS 99%), $Ni(CH_3COO)_2$ (Alfa Aesar 99%) and $Co(CH_3COO)_2$ (PANREAC 99%). After combustion, the materials were calcined at 500°C for 2 h, to assure the total organic removal, annealed at 800ºC for 2 h (NiO-SDC and SDC), and 900ºC for 2 h (LSCF), and ball-milled for 24 h. All powders were characterized by BET and XRD in order to confirm their quality. The XRD patterns of NiO-SDC, SDC and LSCF powders presented no evidences of secondary phases (**Fig. 1**). Finally, BET analysis of NiO-SDC, SDC and LSCF determined specific surface areas of 20-30, 27, and 14 m^2/g, respectively.

2.2 Cell manufacturing

The composition of the microtubular SOFCs were selected as follows: NiO-SDC (60:40 wt.%) as the anode tubular support, NiO-SDC (50:50 wt.%) as the anode functional layer (AFL), SDC as the electrolyte and LSCF-SDC (70:30 wt.%) as the cathode. Three cell configurations, named as cells A, B and C, varying the wall thickness-(outer

diameter) and porosity of tubular supports were processed (**Table 1**). Since the most important parameters of anode supports in mT-SOFCs (within outer diameter range of 1 and 5 mm) on the cell performance are the wall thickness and the porosity, the outer diameter of cells was conditioned to the dimension of wall thickness and formability **[31]**. Thus, cells A and B, without and with added porosity in the support, respectively, presented a wall thickness of ~400 μm (~2.5 mm outer diameter). Cell C exhibited a wall thickness of ~1200 μm (~4.5 mm outer diameter) and with added porosity.

Tubular supports were prepared by the aqueous gel-casting method as described elsewhere **[27,28]**. As mentioned above, a sucrose amount of 0-15 wt.% vs. NiO-SDC was added as pore former, modifying the rheology of the suspensions with respect to previous works. For that reason, it was necessary to adjust the agarose and NiO-SDC powder contents in order to achieve a suitable suspension. According with previous studies, the explored ranges for the different processing parameters were: NiO-SDC solid loading amount of 26-34 wt.% vs. water, commercial dispersant concentration (DOLAPIX GmbH & Co) of 0.75-1.5 wt.% vs. NiO-SDC powder, and agarose content (Lab. Conda) of 0.8-1.2 wt.% vs. the suspension. In order to obtain a homogeneous slurry, the agarose suspension was firstly activated by heating around 80-90ºC, and then kept above 40ºC until casting in order to avoid premature gelation. The formulation of each studied suspension was adjusted to obtain a suitable viscosity for gel-casting, which was between 1500 and 2500 mPa·s at 40ºC and a constant shear rate of 100 s^{-1} using a rheometer (RST CPS. Brookfield 3000). The tubes were formed using a new and simple wet-forming technique based on gel-casting, operating as a syringe **[27]**. For this purpose, a steel punch (Ø = 3 for the cells A and B, and 4 mm for the cell C) with an in-house-designed aluminium die (Ø = 6 for the cells A and B, and 9 mm for the cell C, and length = 200 mm) were used. The resulting green tubes were finally dried in air for 48 h, and cut to a length of 100 mm.

After this, an anode functional layer (composition of 50:50 wt.% NiO-SDC and thickness range of 10-20 μm) was deposited by colloidal spray-coating onto the tubular substrates. The inks consisting of NiO-SDC as solid loading and terpineol as solvent (1:5 wt.%), were prepared to possess low viscosity, high volatility, and moderate solid loading. In order to avoid mechanical degradation of the cell components during the co-sintering process, it was necessary to determine the shrinkage behaviour of the different cell components. For this purpose, an estimation was obtained from the shrinkage curves of NiO-SDC tubular supports and a compact pellet of SDC powder made by the uniaxial pressing method (100 MPa). The linear shrinkage curves were determined using a dilatometer (LINSEIS L75 PT Horizontal) heating at 1 °C·min^{-1} up to 1500 °C. From the shrinkage curves, the AFL and NiO-SDC supports of the tubular half-cells were pre-sintered in air.

Subsequently, SDC electrolyte layers were deposited by colloidal spray-coating, which was also made by mixing commercial SDC with small amounts of cobalt oxide (2.0 wt.%) used as a sintering aid, and terpineol (1:5 wt./wt.) as a organic solvent. Then, both anode and electrolyte layers were co-sintered at 1450°C for 5 h. After co-sintering, 70:30 wt.% LSCF-SDC cathode precursor were also mixed with terpineol (1:5 wt.%) to make a colloidal suspension, and sprayed onto the half-cell, and finally sintered at 1050°C for 2 h in air.

Final cell dimensions were: 2.6 mm (cells A), 2.4 mm (cell B) and 4.5 mm (cell C) of outer diameters, 70-80 mm length with cathode active areas of 65, 60 and 100 mm^2 for cells A, B and C, respectively. Microstructures of the cell components were analyzed by scanning electron microscopy (SEM). After reducing process (NiO to Ni at the anode), the total porosity of supports was determined using a helium gas absorption pycnometer (Micromeritics ASAP2000).

2.3 Electrochemical characterization

Three replicates of each cell configuration were electrochemically tested using humidified H_2 as fuel in the anodic compartment and air in the cathodic chamber. Electrical connections were made using four Ag wires. Ag mesh was used as current collector at the anode (inner of the tube) and coiled Ag wire fixed with Ag paste was used at the cathode side. Tubes were sealed using Ceramabond 503 sealant (Aremco, US) into alumina tubes and finally all the system was kept into a quartz tube, and sealed again to separate both chambers. Additional details of the experimental setup can be found in previous works [32,33]. The cell was heated up to 700ºC in a small tubular furnace under nitrogen (100 ml/min) at the anode chamber and static air at the cathode side. At this temperature, humidified hydrogen (100 ml/min) was introduced to firstly reduce the anode and then to operate the cell. Electrochemical measurements were carried out at intermediate temperature between 600ºC and 650ºC. j-V (current density- Voltage) and AC impedance measurements were recorded using a VSP Potentiostat/Galvanostat (Princeton Applied Research, Oak Ridge, US). Electrochemical impedance spectroscopy (EIS) measurements were performed using a sinusoidal amplitude signal of 50 mV in the frequency range of 500 kHz to 10 mHz. EIS experimental data was fitted using an equivalent circuit model with the following components: L corresponds to an inductance, which is usually associated with the current/voltage probes, or to the high-frequency phase shift of the electrochemical equipment; R_{ohm} is the ohmic resistance; (R1, CPE1) and (R2, CPE2) correspond to the high- and intermediate-frequency arcs, respectively, and W_3 is a finite Warburg element associated to diffusion processes [34].

3 Results and discussion

3.1 Formulation of suspensions

Table 2 shows the different formulations of suspensions for the gel-casting system of the different cells. A dispersant content of 1.0 wt.% vs. NiO-SDC powder was suitable to disperse the NiO-SDC powder in distilled water. Formulation 3 (for cell A) and 9 (for cells B and C) were selected as the most suitable suspensions for gel-casting of the cell supports. Formulation 9 presents the maximum amount in solid loading (34 wt.% powder/water) and the minimum content in agarose (1.00 wt.% agarose/suspension) for a pore former amount of 10 wt.% sucrose/solid loading. Formulation 3 also shows the maximum solid loading (34 wt.% powder/water) and the minimum content in agarose (0.90 wt.% agarose/suspension) for 0 wt.% sucrose/solid loading. Thus, cast green bodies with enough mechanical strength during drying, pre-sintering and co-sintering process are obtained. In addition, a formulation with a high solid loading is interesting in order to minimize the shrinkage of the supports during drying and sintering processes. However, higher solid loadings (> 34 wt.%) are not suitable for casting, as the high viscosity of the suspensions became difficult to fill the mould, generating macroscopic defects in the green bodies. In addition, the formulation with 15 wt.% sucrose/solid loading was dismissed, due to a low mechanical strength of the cells.

3.2 Optimization of pre-sintering process

Shrinkage curves of different NiO-SDC tubular supports and the SDC electrolyte are shown in **Fig. 2**. The large difference in shrinkage between both materials evidences that a pre-sintering process of the tubular supports with their AFLs is necessary to decrease their shrinkages during co-sintering. In addition, the electrolyte material shrinks faster than the tubular supports, enhancing the densification of the electrolyte layers. Pre-sintering temperatures of 1000ºC for cell A, and 1100ºC for cells B and C are appropriate to obtain an anode-support shrinkage of 11, 16 and 15%, respectively, which is close to the shrinkage difference between the support and SDC layer during co-sintering at 1450ºC.

3.3 Microstructure of mT-SOFCs

Figs. 3 (a-c) exhibit the microstructures of the different supports consisting of Ni and SDC, after reducing in H_2, which were processed with different sucrose amounts. The supports presented porosities of 39, 54 and 57% for the cells A, B and C. The support with 15 wt.% sucrose, and a porosity of 62%, was finally dismissed due to its low mechanical strength and low dimensional stability. Therefore, both cells B and C were fabricated using 10 wt.% of sucrose. **Figs. 3 (d-f)** show the transverse cross-sectional microstructure of cells, which present thicknesses around 15 μm for the AFL, and 15 μm for the electrolyte. They also evidence that the interfaces between the electrolyte and the electrodes exhibits no observable delamination or cracks. After co-sintering the anode supports are homogeneous presenting high porosity, and the electrolyte layers present high density. In addition, the anode functional layer contributes to a progressive gradation in porosity between the support and the electrolyte.

3.4 Electrochemical characterization

OCVs for the replicates of three cell configurations are around 0.73 at 600ºC and 0.68 V at 650ºC (**Table 3**). These values are lower than those predicted from the Nernst equation, under H_2 as a fuel and air as an oxidant. Similar OCV behaviour has been reported by other authors using doped ceria electrolytes for mT-SOFCs. Suzuki et al. **[35,36]** worked with anode-supported needle-type micro SOFCs, with a needle-type cell diameter of 0.4 mm and a GDC electrolyte thickness around 10 μm. For that geometry, the OCV decreased from 0.89 to 0.83 V with increasing the operating temperature from 450 to 550ºC. However, the open circuit voltage increased up to 0.96 V when the thickness of the electrolyte increased to 30 μm and the anode was fabricated less permeable for gases. The same problem was also reported by Yamaguchi et al. **[37]** working with an anode-supported microtubular SOFC of 1.5 mm

diameter and 15 μm GDC electrolyte layer. In this case, OCV values were below 0.90, 0.84 and 0.77 V at 450, 500 and 550ºC, respectively. In the present work, the decrease in the OCV is partially caused by gas leakages between anode and cathode chambers, due to the presence of small pores at the electrolyte layer (**Fig. 4**). It could also be associated to the internal short circuit currents due to the increase of electronic conductivity in the doped ceria electrolyte **[38,39]**. Finally, it is also well known that the solubility of cobalt oxide, used as a sintering aid, in the fluorite structure is very low and the excessive cobalt oxide segregates as layer of a few nanometers at the grain boundaries, which could introduce (additional to the reduction from Ce^{4+} to Ce^{3+}) n-type electronic conductivity with increasing temperature and decreasing oxygen partial pressure. As the electronic conductivity of doped-ceria and sintering aid intrinsically depend on the electrolyte material, they probably influenced on the performance of the cells in a similar way. The relatively good reproducibility in OCVs and ASRs of the replicated cells, with differences of about 5%, indicates that the amount of pores in the electrolyte of each cell configuration could possibly justify those differences. In order to avoid the effect of these gas leakages and the internal short circuit current, it will be necessary to develop cells free of small pores and possibly thicker layers.

Fig. 5 shows the *j*-V (current density vs. cell voltage) and *j*-P curves (current density vs. power density) for the different cells. *j*-V curves exhibited a slightly unstable behaviour with oscillations, due to the presence of small gas leakages through micro-pores at the electrolyte layer. Despite this phenomenon, maximum power densities of 220, 400 and 180 mW·cm^{-2} at 650°C were achieved for the cells A, B and C, respectively. Despite the low operation voltage, these performances, operating in the temperature range of 600-650ºC (**Table 3**), are comparable to those of anode-supported microtubular SOFCs with diameters of 0.8-6.0 mm, active cell areas higher than 50 mm^2 and doped-ceria electrolyte layers (350-600 mW·cm^{-2} operating between 500 and 650ºC) reported by other authors **[31,35,37,40,41,42]**. The difference in power output between cells A

and B evidence the significant effect of the porosity of the support on their performances. These results also reveal the strong influence of support thicknesses, which are 380 and 1200 μm for the cells B and C, respectively. In addition, concentration polarization is clearly observed from cell C at high current densities, due to the thicker anode support. From those results, it was confirmed that cell B (with increased porosity and smaller wall thickness at the support) achieved the higher current densities, indicating good gas diffusion at the support and an adequate catalytic activity at both electrodes. In addition, the area specific resistances (ASRs) for the cells, determined from the slopes of the j-V curves, are shown in **Table 3**. Those values are in the range of other reported results in the literature.

EIS experiments under OCV conditions at 600ºC were also performed as shown in **Fig. 6.** Due to the presence of small pores at the electrolyte layer and as a consequence lowering the OCV as previously discussed, EIS recorded data was slightly noisy, especially at lower frequencies. In spite of this, the experimental data was fitted using equivalent circuits and a summary of the obtained parameters is shown in **Table 4**. Firstly, R_{ohm} values are higher than those expected for a 15 µm thick SDC electrolyte, possibly due to insufficient density of the electrolyte in the three cells. Assignation of the different contributions is usually complex, although some valuable conclusions can be deduced from this data. Low frequency Warburg response (W_3) is assigned to a diffusion process, in this case to hydrogen transport through the Ni-SDC support. This assignation is consistent, as higher values (0.83 $\Omega \cdot cm^2$) were found for Cell C (thicker support). In addition, for identical wall thickness, lower values (0.10 $\Omega \cdot cm^2$) were obtained for Cell B (containing extra porosity) in comparison with Cell A (no extra porosity, 0.18 $\Omega \cdot cm^2$). Intermediate frequency component (R_2) is almost constant for the three studied cells. In addition, this component was varying when switching from air to oxygen atmosphere, while the rest of the components remained constant. For that reason R_2 was assigned to the cathode activation. Finally, assignation of the high

frequency component (R_1) is not clear, although it was tentatively associated with anode activation **[43]**. The observed capacitance values do not suffer significant variation for the different studied cells, and their values are consistent with similar microtubular cells reported in the literature [44]. Finally, ASR values obtained from EIS data (**Table 3**) are significantly higher with those obtained from the j-V curves (**Table 2**), as a consequence of the activation polarization of the cells, which takes place at low current densities. In addition, gas leakage will increase cell temperature especially at higher current densities and as a consequence, lower ASR values are observed from j-V experiments.

Fig. 7 shows the post-mortem AFL-support microstructure for the three cells after testing for 15 h. The uniform sponge-like porous structure at the support of cell B and its reduced thickness is suitable for mT-SOFCs, as large pores provide a path with low resistance to rapid gas transport. In addition, small pores at the AFL are expected to provide a large number of Triple Phase Boundaries (TPBs) for the electrochemical reactions.

4 Conclusions

Micro-tubular SOFCs with ~2.5 and ~4.5 mm outer diameters, and ~400 and ~1200 μm wall thicknesses, respectively, were fabricated using a simple wet-forming method based on agarose gel-casting technique, which operates as a syringe. Suitable slurry formulations for gel-casting were prepared, without and with (10 wt.% sucrose) added pore former. Pre-sintering temperature of supports was optimized from linear shrinkage curves, thus obtaining a dense electrolyte without anode-electrolyte delamination after co-sintering. Electrochemical tests showed the highest power density (400 mW·cm^{-2} at 650°C) for cell B, presenting 380 μm wall thickness (2.4 mm outer diameter), and added porosity using 10 wt.% sucrose. The high current density for this cell evidences

good gas diffusion at the tubular supports. In contrast, cell A (220 mW·cm^{-2}) with a tubular support close to cell B and without added porosity, and cell C (180 mW·cm^{-2}) with one of 1200 μm thickness and added porosity presented lower performances than cell B. These results indicate that the support thickness and porosity of anode-supported mT-SOFCs is strongly influenced on the cell performance. The relatively low OCVs (0.73-0.68 V at 600-650ºC) are probably due to the current leakage related to the electronic conduction and the presence of small gas leakages through micro-pores at the electrolyte layer. As a summary, the aqueous agarose gel-casting method operating as a syringe, combined with additional porosity and thickness reduction of the support, is a suitable processing route to enhance the performance of anode-supported mT-SOFCs.

Acknowledgements
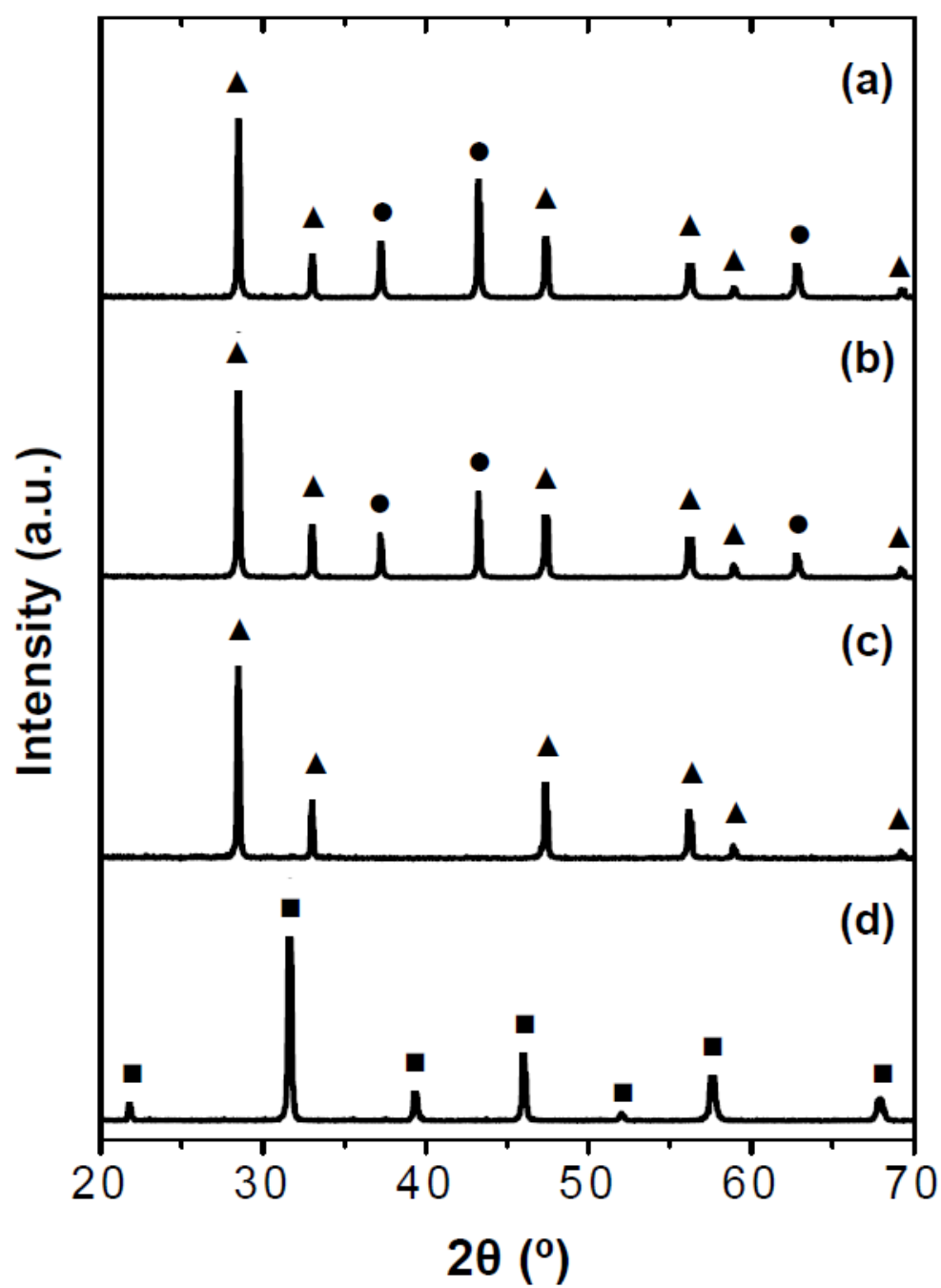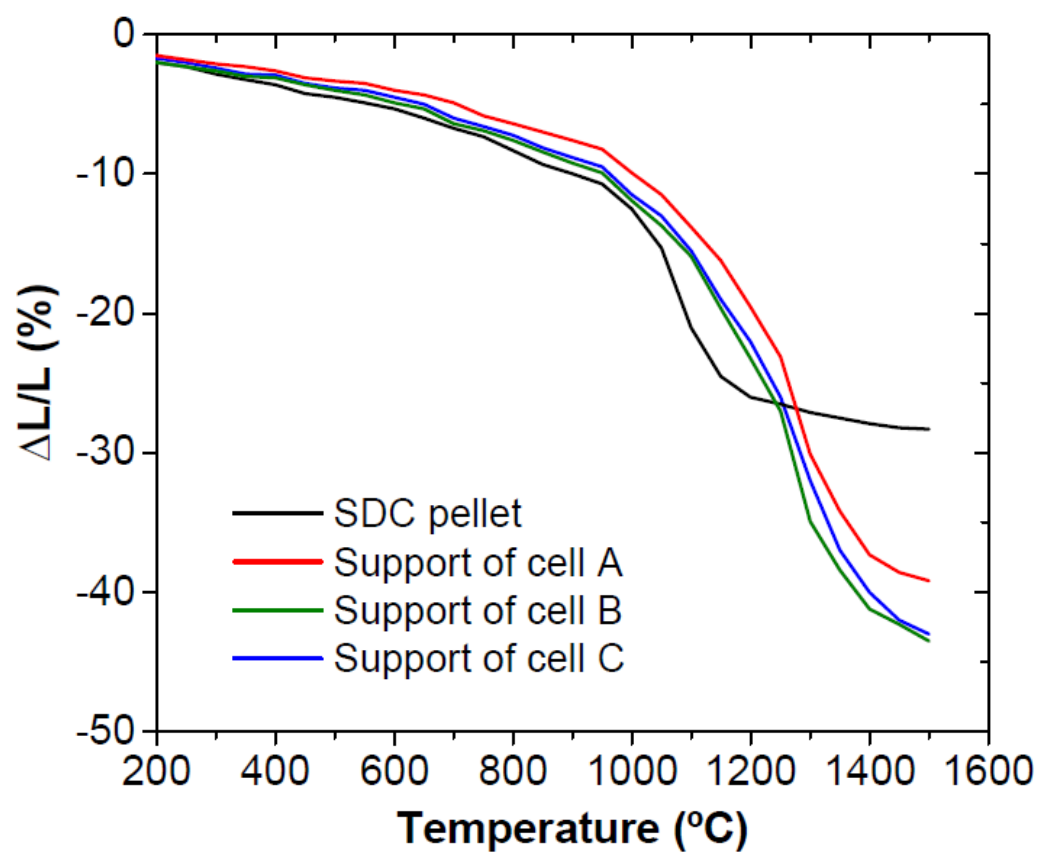
Figure 1

Figure 2

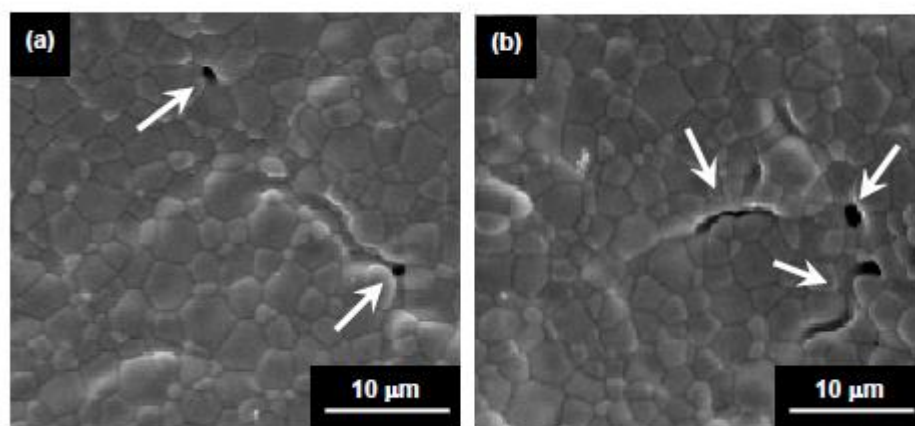Figure 3
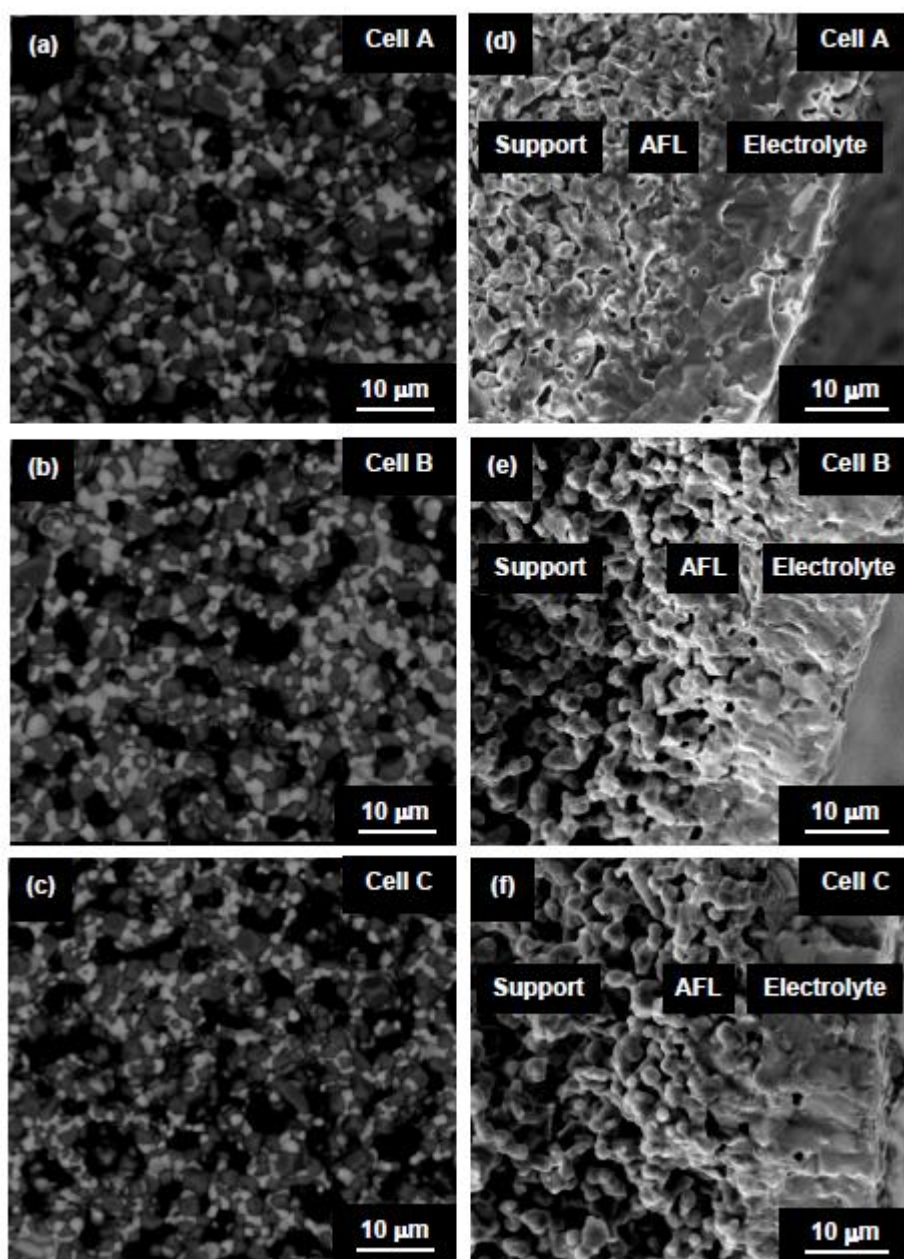
Figure 4

Figure 5
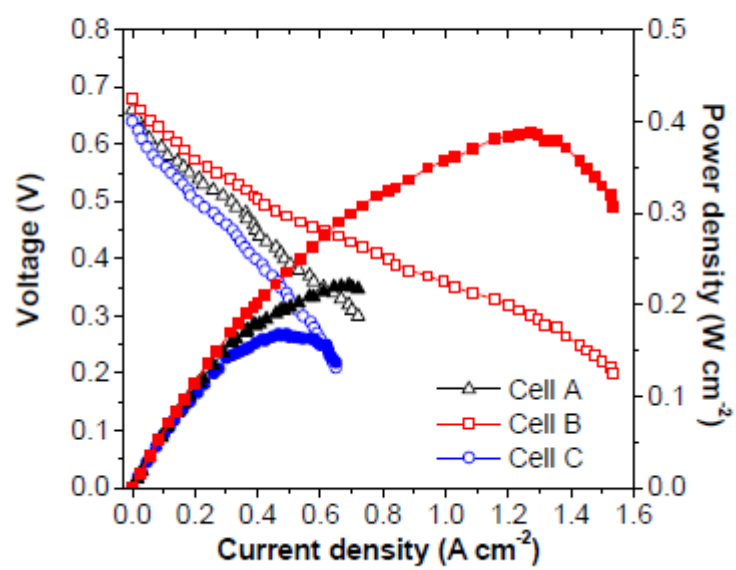
Figure 6
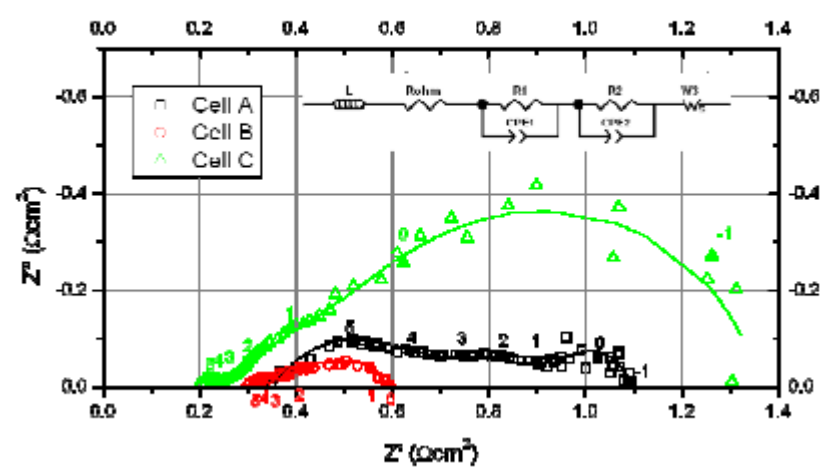
Figure 7
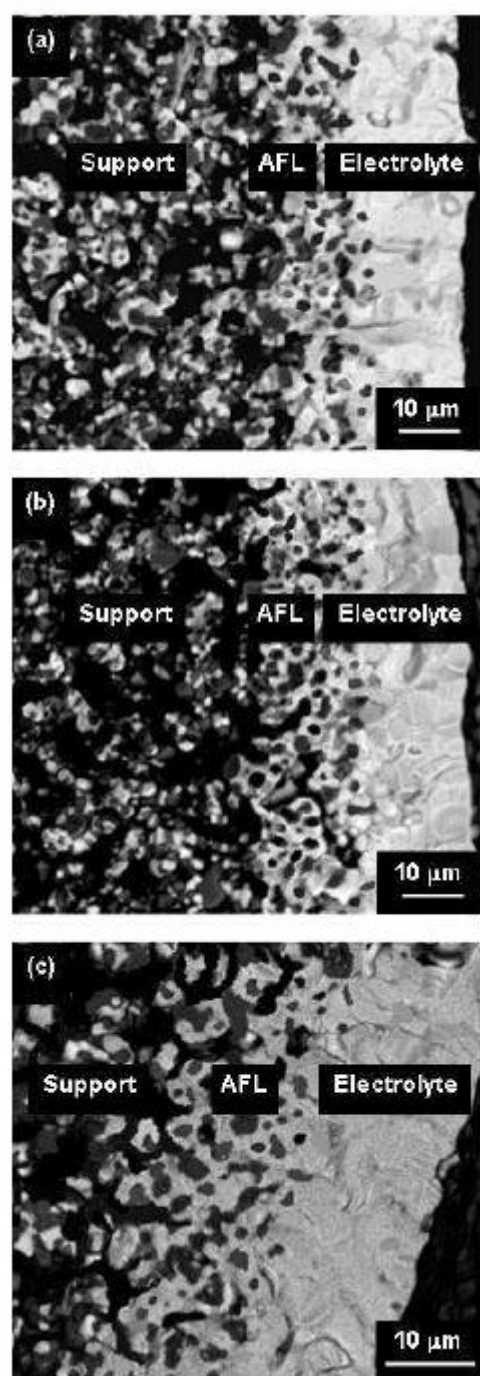
Table 1

Cell	Wall thickness–(Outer diameter) (μm) (mm)	Pore former
A	400 – (2.6)	No
B	380 – (2.4)	Yes
C	1200 – (4.5)	Yes

Table 2

Formulation (N°)	Solid loading (wt.% vs. water)	Sugar (wt.% vs. solid loading)	Agarose (wt.% vs. suspension)	Observations
1	26	0	1.05	Plastically deformed during handling and by its own weight
2	30	0	1.00	Suitable mechanical strength during handling and after sintering.
3	34	0	1.00	
4	26	5	1.05	Plastically deformed during handling and by its own weight.
5	30	5	1.00	Suitable mechanical strength during handling and after sintering.
6	34	5	0.95	
7	26	10	1.00	Low mechanical strength after sintering process.
8	30	10	0.95	
9	34	10	0.90	Suitable mechanical strength during handling and after sintering.
10	26	15	0.95	
11	30	15	0.90	Low mechanical strength after sintering.
12	34	15	0.85	

Table 3

Cell	Thickness (μm)	Support porosity (%)	Operating temperature (°C)	OCV (V)	Max. power density (mW·cm^{-2})	ASR (Ω·cm^2)
A	400	40	600	0,72	160	0.85
			650	0,66	220	0.41
B	380	55	600	0,73	280	0.41
			650	0,68	400	0.22
C	1200	55	600	0.69	130	0,84
			650	0.65	180	0,44

References

[1] EG&G Technical Services, Inc., Fuel Cell Handbook (Seventh Edition). University Press of the Pacific, 2004.

[2] P. Aguiar, D.J.L. Brett, N.P. Brandon. J. Power Sources, 171, 2007, 186.

[3] K. Kendall, M. Palin. J. Power Sources 1998, 71, 268.

[4] C.E. Hatchwell, N.M. Sammes, K. Kendall. J. Power Sources 1998, 70, 85.

[5] K. Yashiro, N. Yamada, T. Kawada, J. Hong, A. Kaimai, Y. Nigara, J. Mizuski. Electrochemistry 2002, 70, 958.

[6] T. Suzuki, T. Yamaguchi, Y. Fujishiro, M. Awano. J Power Sources, 2006, 160, 73.

[7] Y.Funahashi, T. Shimamori, T. Suzuki, Y. Fujishiro, M. Awano. J. Power Sources 2007, 163, 731.

[8] X.Y. Zhou, A. Pramuanjaroenkij, S. Kakaç. NATO Science for Peace and Security Series C, Environmental Security (2008) 319-334.

[9] M.Á. Laguna-Bercero, A. Férriz, Á. Larrea, L. Correas, V.M. Orera. Fuel Cells 2013, 13, 1116.

[10] B.C.H. Steele, A. Heinzel. Nature 2001, 414, 345.

[11] V.V. Kharton, F.M.B. Marques, A. Atkinson. Solid State Ionics 2004, 174, 135.

[12] J. Fergus, R. Hui, X. Li, D.P. Wilkinson, J. Zhang. Solid Oxide Fuel Cells: Materials Properties and Performance, CRC, 2008.

[13] M. Morales, J.M. Pérez-Falcón, A. Moure, J. Tartaj, F. Espiell, M. Segarra. Int. J. Hydrogen Energ. 2014, 39, 5451.

[14] V. Gil, J. Gurauskis, R. Campana, R.I. Merino, A. Larrea, V.M. Orera. J. Power Sources 2011, 196, 1184.

[15] T. Mahata, S.R. Nair, R.K. Lenka, P.K. Sinha. Int. J. Hydrogen Energ. 2012, 37, 3874.

[16] A. Mirahmadi, K. Valefi. Ionics 2011, 17, 767.

[17] H. Monzón, M.A. Laguna-Bercero, A. Larrea, B.I. Arias, A. Várez, B. Levenfeld. Int. J. Hydrogen Energ. 2014, 39, 5470.

[18] J.S. Cherng, C.C. Wu, W.H. Chen, T.H. Yeh. Ceram. Int. 2013, 39, S601.

[19] M.H.D. Othman, N. Droushiotis, Z. Wu, G. Kelsall, K. Li. Adv. Mater. 2011, 23, 2480.

[20] A. Douy. Int. J. Inorg. Mater. 2001, 3, 699-707.

[21] A.J. Millán, I. Santacruz, A.J. Sánchez-Herencia, M.I. Nieto, R. Moreno. Adv. Eng. Mater. 2002, 4, 913.

[22] J. Yang, J. Yu, Y. Huang. J. Eur. Ceram. Soc. 2011, 31, 2569.

[23] O.O. Omatete, M.A. Janney, S.D. Nunn. J. Eur. Ceram. Soc. 1997, 17, 407.

[24] C. Fu, S.H. Chan, Q. Liu, X. Ge, G. Pasciak. Int. J. Hydrogen Energ. 2010, 35, 301.

[25] D. Dong, J. Gao, X. Liu, G. Meng. J. Power Sources 2007, 165, 217.

[26] M.A. Janney, O.O. Omatete, C.A. Walls, S.D. Nunn, R.J. Ogle, G. Westmoreland. J. Am. Ceram. Soc. 1998, 81, 581.

[27] M.E. Navarro, X.G. Capdevila, M. Morales, J.J. Roa, M. Segarra. J. Power Sources 2012, 200, 45.

[28] M. Morales, M.E. Navarro, X.G. Capdevila, J.J. Roa, M. Segarra. Ceram. Int. 2012, 38, 3713.

[29] M. Morales, J.J. Roa, X.G. Capdevila, M. Segarra, S. Piñol. Fuel Cells 2011, 11, 108.

[30] M. Morales, J.J. Roa, J. Tartaj, M. Segarra. J. Power Sources 2012, 216, 417.

[31] V. Lawlor. J. Power Sources 2013, 240, 421.

[32] M.A. Laguna-Bercero, R. Campana, A. Larrea, J.A. Kilner, V.M. Orera. Fuel Cells 2011, 11, 116.

[33] M.A. Laguna-Bercero, R. Campana, A. Larrea, J.A. Kilner, V.M. Orera. J. Electrochem. Soc. 2010, 157, B852.

[34] Impedance Spectroscopy, 2nd Edition, Eds. E. Barsoukov & J. Ross Macdonald, John Wiley & Sons, Hoboken, NJ, 2005.

[35] T. Suzuki, Y. Funahashi, Z. Hasan, T. Yamaguchi, Y. Fujishiro, M. Awano. Electrochem. Commun. 2008, 10, 1563.

[36] T. Suzuki, Y. Funahashi, T. Yamaguchi, Y. Fujishiro, M. Awano. Solid State Ionics 2009, 180, 546.

[37] T. Yamaguchi, T. Suzuki, S. Shimizu, Y. Fujishiro, M. Awano. J. Membr. Sci. 2007, 300, 45.

[38] D.P. Fagg, J.C.C. Abrantes, D. Pérez-Coll, P. Núñez, V.V. Kharton, J.R. Frade. Electrochim. Acta 2003, 48, 1023.

[39] D. Perez-Coll, P. Nunez, J.C.C. Abrantes, D.P. Fagg, V.V. Kharton, J.R. Frade. Solid State Ionics 2005, 176, 2799.

[40] T. Suzuki, T. Yamaguchi, Y. Fujishiro, M. Awano. J. Power Sources 2006, 160, 73.

[41] S.-Y. Park, C. Woong Na, J.H. Ahn, U.-J. Yun, T.-H. Lim, R.-H. Song, D.-R. Shin, J.-H. Lee. J. Power Sources 2012, 218, 119.

[42] K.S. Howe, G.J. Thompson, K. Kendall. Journal of Power Sources 2011, 196, 1677.

[43] R. Campana, R.I. Merino, A. Larrea, I. Villarreal, V.M. Orera. J. Power Sources 2009, 192, 120.

[44] M.A. Laguna-Bercero, Amir R. Hanifi, Hernan Monzon, Joshua Cunningham, Thomas H. Etsell and Partha Sarkar, J. Mater Chem. A. 2014, 2, 9764.